KICS The Korean Institute of Communications and Information Sciences

Available online at www.sciencedirect.com

ScienceDirect

ICT Express 5 (2019) 235–239

www.elsevier.com/locate/icte

Interference modeling and analysis in 3-dimensional directional UAV networks based on stochastic geometry

Eunmi Chu[a], Jong Min Kim[b], Bang Chul Jung[a,*]

[a] *Department of Electronics Engineering, Chungnam National University, Daejeon, South Korea*
[b] *Korea Science Academy of KAIST, Busan, South Korea*

Received 30 August 2019; accepted 16 September 2019
Available online 8 October 2019

Abstract

In this paper, we model and characterize interference of directional unmanned aerial vehicle (UAV) networks based on stochastic geometry, where each UAV is equipped with a directional antenna and it communicates with another UAV that is located in the three dimensional (3D) space. In particular, the 3D location of UAVs is assumed to be uniformly distributed in a certain volume, which is modeled by Poisson point process. Given a beamwidth, we first design an ideal 3D directional antenna beam pattern with a constant gain of both main-lobe and side-lobe. To model the interference in the UAV network, we analyze the effect of elevation and azimuth between a typical UAV receiver and an interfering UAV transmitter with spherical coordinate system. Then, we investigate distribution of the aggregate interference at a typical UAV receiver from multiple UAVs in terms of side-lobe gain, beamwidth, height of UAV, and distance of a UAV transmitter–receiver pair.

Keywords: UAV networks; Poisson point process (PPP); 3D directional antenna; Interference; Stochastic geometry

1. Introduction

Recently, an unmanned aerial vehicles (UAV) communication has widely been investigated with various applications due to its low cost of deployment and rapid stabilization of networks. In general, the UAV applications include real-time monitoring of road traffic, remote sensing, disaster communications, product delivery, precision agriculture, etc [1]. Most studies on the UAV communication have focused on performance improvement for terrestrial wireless networks. A framework of UAV-assisted vehicular network was introduced in [2], where it was shown that various performance metrics such as connectivity, infrastructure coverage, network information collection ability, and network interworking efficiency can be improved by cooperating the UAVs and terrestrial communication infrastructure. In [3], coverage probability at a ground user in the UAV-assisted network where multiple UAVs are assumed to be located in a three-dimensional (3D) space and they are assumed to move based on the mixed random waypoint mobility model. In [4], a tight lower bound for the outage probability as well as the optimal UAV height for a given air-to-ground link are analytically derived. In [5], a cooperative data dissemination framework was proposed in air-ground integrated networks to maximize the minimum received data amount of ground users, where a terrestrial base station and a single UAV cooperatively serve ground users. In [6], the 3D air–ground channel and 3D antenna patterns between the ground base station and UAV are utilized for more accurate analysis.

Different from UAV-assisted terrestrial wireless networks, a communication among UAVs has not received much attention from both academia and industry due to relatively rare applications and hash technical challenges such as highly mobility of UAVs and frequent topology changes. However, a network consisting of multiple UAVs which are connected by air-to-air wireless channels has recently been investigated due to the increase in the deployment of UAVs. In [7], a novel directional medium access control (MAC) protocol was proposed to coordinate transmissions of many UAVs, equipped with directional antennas, in 3D space. Furthermore, an mmWave-enabled UAV swarm network was studied for massive data exchange among UAVs in [8], where a 3D interference graph was

* Corresponding author.
E-mail addresses: emchu@cnu.ac.kr (E. Chu), franzkim@kaist.ac.kr (J.M. Kim), bcjung@cnu.ac.kr (B.C. Jung).

Peer review under responsibility of The Korean Institute of Communications and Information Sciences (KICS).

https://doi.org/10.1016/j.icte.2019.09.006

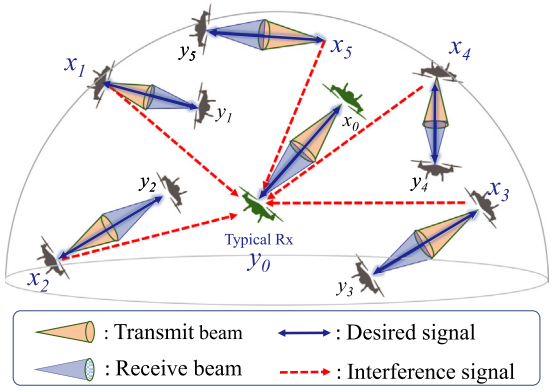

Fig. 1. Directional UAV networks.

exploited by considering mobility, interference, and energy consumption simultaneously.

As the UAV network become denser, the interference among UAV wireless links tends to limit the network performance and thus it is important to analyze the interference characteristics of the UAV network in 3D space as shown in Fig. 1. Existing studies only focused on a simple 3D wireless network without considering the effect of side-lobe of the directional antennas. In our previous paper [9], we shortly described an ideal 3D directional antenna model considering the effect of side-lobe and then analyze the interference characteristics of the directional UAV network where UAVs are randomly located in 3D space according to Poisson Point Process (PPP).

In this paper, we describe an ideal 3D directional antenna model and a network model in detail. Additionally, we investigate distribution of the aggregate interference at a typical UAV receiver from multiple UAVs in terms of side-lobe, beamwidth, the height of UAV and the distance of a pair of UAV communicating each other.

2. Interference modeling

2.1. Directional antenna model in 3D space

In the ideal omni antenna, the radiation pattern is uniformly radiated to the area of the isotropic sphere. When the radius of sphere is set to 1, surface area $\mathcal{A}_o$ is to be 4π. Since the energy source power $\mathcal{P}_o$ is radiated on $\mathcal{A}_o$, radiation intensity G_o represents the power radiated from an antenna per unit sphere and it is expressed as follows:

$$G_o = \frac{\mathcal{P}_o}{\mathcal{A}_o}, \tag{1}$$

Assuming that G_o is 1, then $\mathcal{P}_o$ is to be 4π.

In contrast, in the directional antenna, the radiation pattern is consisted of a main-lobe and a side-lobe. Energy source power is separated by the main-lobe and the side-lobe. In directional antenna, the energy source of the omni antenna $\mathcal{P}_o$ is expressed as follows:

$$\mathcal{P}_o = \mathcal{P}_m + \mathcal{P}_s, \tag{2}$$

where $\mathcal{P}_m$ and $\mathcal{P}_s$ denote the radiated energy on the areas of the main-lobe and side-lobe, respectively. Samely, total surface area of omni-antenna is separated to the surface area of main-lobe and side-lobe as follows:

$$\mathcal{A}_o = \mathcal{A}_m + \mathcal{A}_s, \tag{3}$$

where $\mathcal{A}_m$ and $\mathcal{A}_s$ denote the surface area of main-lobe and side-lobe, respectively.

Accordingly, the radiation density of main-lobe G_m and the radiation density of side-lobe G_s is expressed as follows:

$$G_m = \frac{\mathcal{P}_m}{\mathcal{A}_m}(\text{main-lobe}),\ G_s = \frac{\mathcal{P}_s}{\mathcal{A}_s}(\text{side-lobe}). \tag{4}$$

Since $\mathcal{A}_m$ is determined by the beamwidth ω, $\mathcal{A}_m(\omega)$ is used instead of $\mathcal{A}_m$ as follows:

$$\mathcal{A}_m(\omega) = \int_{\rho=0}^{\omega}\int_{\phi=0}^{\omega} \sin\phi\, d\phi\, d\rho, (\text{main-lobe}), \tag{5}$$

where ρ and ϕ denote azimuth and elevation in a spherical coordinate system, respectively. Similarly, for given ω, the radiation intensity of main-lobe is expressed as follows:

$$G_m(\omega) = \frac{\mathcal{P}_m(\omega)}{\mathcal{A}_m(\omega)}, (\text{main-lobe}). \tag{6}$$

The side-lobe is usually radiated to the opposite direction form the main-lobe. It wastes energy and may cause interference to other equipment. All practical antennas incur a certain amount of side-lobe although ideal antennas have zero side-lobe. Let G_s be the radiation intensity of side-lobe, it is expressed as follows:

$$G_s = \frac{\mathcal{P}_s}{\mathcal{A}_s} = \frac{\mathcal{P}_o - \mathcal{P}_m(\omega)}{\mathcal{A}_o - \mathcal{A}_m(\omega)}, (\text{side-lobe}), \tag{7}$$

where the denominator is applied by Eqs. (3) and (5), and the nominator is applied by Eq. (2).

The energy source power of main-lobe for a given ω is calculated from Eq. (7) as follows:

$$\mathcal{P}_m(\omega) = \mathcal{P}_o - G_s\left(\mathcal{A}_o - \mathcal{A}_m(\omega)\right). \tag{8}$$

Therefore, since the gain of main-lobe is calculated by given ω and G_s, $G_m(\omega)$ is replaced to $G_m(\omega, G_s)$ as follows

$$G_m(\omega, G_s) = \frac{G_o\mathcal{A}_o - G_s\left(\mathcal{A}_o - \mathcal{A}_m(\omega)\right)}{\mathcal{A}_m(\omega)}. \tag{9}$$

In reality, the values of G_m and G_s are varied depending on the arrival angles. However, for simplicity, we assume an ideal directional antenna gain pattern which are consisted of two constant values of G_s and G_m in this paper.

2.2. Network model in 3D space

We consider a 3-dimensional UAV network where simultaneously transmitting UAVs are distributed as PPP $\Gamma = \{\mathbf{x_1}, \mathbf{x_2}, \ldots\}$ on $\mathbb{R}^3$. Assuming that a terrestrial area is A and intensity of the UAV on 2-dimensional terrestrial area is λ, the number of UAVs of λA is distributed on the 3-dimensional UAV network, i.e., the cardinality of Γ is λA. We denote $\mathbf{y_i}$ as a receiving UAV corresponding to a transmitting UAV $\mathbf{x_i}$. We assume that the pair of $\mathbf{x_i}$ and $\mathbf{y_i}$ is perfectly aligned toward the

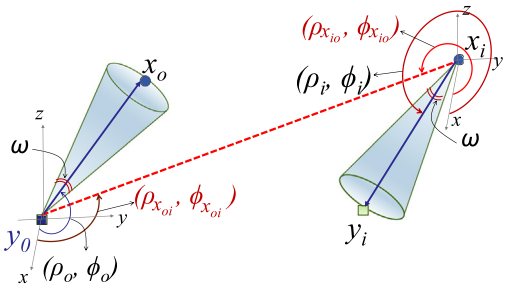

Fig. 2. UAV's antenna gain model.

center direction of beamwidth ω. The distance between $\mathbf{x_i}$ and $\mathbf{y_i}$ is d_i which is randomly and uniformly determined within the range of the minimum distance of d_{min} and the maximum distance of d_{max}. The value on z-axis of $\mathbf{x_i}$, i.e., the height of UAV h_{xi} also is randomly and uniformly determined within the range of the minimum height of h_{min} and the maximum height of h_{max}.

In summary, $\mathbf{x_i}$ and $\mathbf{y_i}$ are randomly and uniformly generated along with the following conditions:

$$\begin{aligned}&\mathbf{x_i} = (a_{xi}, b_{xi}, h_{xi}),\ \mathbf{y_i} = (a_{yi}, b_{yi}, h_{yi}) \text{ on } \mathbb{R}^3,\\ &\quad where \quad \|\mathbf{x_i} - \mathbf{y_i}\| = d_i,\\ &\qquad\quad d_{min} \le d_i \le d_{max},\\ &\qquad\quad h_{min} \le h_{xi} \le h_{max},\\ &\qquad\quad h_{min} \le h_{yi} \le h_{max}.\end{aligned}$$

A typical receiver $\mathbf{y_o}$ is located in the center of an observing target area, and the pair of $\mathbf{x_o}$ and $\mathbf{y_o}$ also retains the distance R. To easily calculate antenna gain, we translate the cartesian coordinate system into the spherical coordinate system. Elevation ϕ is the angle between the vector of r and the z-axis whereas azimuth ρ is the angle between x-axis and the projection of the vector r on the xy plane as shown in Fig. 2. The angles $(\rho_{x_{io}}, \phi_{x_{io}})$ and $(\rho_{x_{oi}}, \phi_{x_{oi}})$ are generated by a vector of $(\mathbf{x_i}, \mathbf{y_o})$ and a vector of $(\mathbf{y_o}, \mathbf{x_i})$, respectively. Likewise, the angles (ρ_o, ϕ_o) and (ρ_i, ϕ_i) are generated by their pairs, i.e., a vector of $(\mathbf{y_o}, \mathbf{x_o})$ and a vector of $(\mathbf{x_i}, \mathbf{y_i})$.

Transmit antenna gain at the typical node $\mathbf{y_o}$ from interference node $\mathbf{x_i}$ is expressed as follows:

$$\mathcal{G}_t\left(\rho_{x_{io}}, \phi_{x_{io}}, \omega, G_s\right) = \begin{cases} G_m(\omega, G_s), & \text{if } \left(\rho_{x_{io}} \in \overrightarrow{\Psi}_i\right) \cap \left(\phi_{x_{io}} \in \overrightarrow{\Phi}_i\right), \\ G_s, & \text{otherwise,}\end{cases} \tag{10}$$

where $\overrightarrow{\Psi}_i$ and $\overrightarrow{\Phi}_i$ denote set of angles of main-lobe for a pair of $\mathbf{x_i}$ and $\mathbf{y_i}$, i.e., $\overrightarrow{\Psi}_i = \left[\rho_i - \frac{\omega}{2}, \rho_i + \frac{\omega}{2}\right]$ and $\overrightarrow{\Phi}_i = \left[\phi_i - \frac{\omega}{2}, \phi_i + \frac{\omega}{2}\right]$.

Receiver antenna gain at the typical node $\mathbf{y_o}$ from interference node $\mathbf{x_i}$ is expressed as follows:

$$\mathcal{G}_r\left(\rho_{x_{oi}}, \phi_{x_{oi}}, \omega, G_s\right) = \begin{cases} G_m(\omega, G_s), \text{ if } \left(\rho_{x_{oi}} \in \overleftarrow{\Psi}_i\right) \cap \left(\phi_{x_{oi}} \in \overleftarrow{\Phi}_i\right), \\ G_s, \qquad\qquad \text{otherwise,}\end{cases} \tag{11}$$

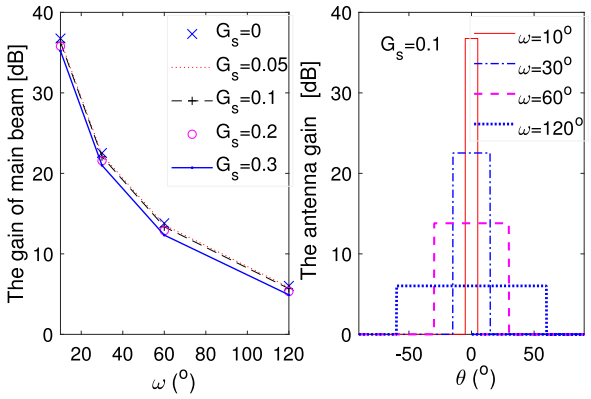

Fig. 3. Simplified antenna model of G_m and G_s for ω.

where $\overleftarrow{\Psi}_i$ and $\overleftarrow{\Phi}_i$ denote angle of main-lobe for a pair of $\mathbf{x_o}$ and $\mathbf{y_o}$, i.e., $\overleftarrow{\Psi}_i = \left[\rho_o - \frac{\omega}{2}, \rho_o + \frac{\omega}{2}\right]$ and $\overleftarrow{\Phi}_i = \left[\phi_o - \frac{\omega}{2}, \phi_o + \frac{\omega}{2}\right]$.

Therefore, the received desired signal $\mathcal{S}$ and the interference signal I at the typical receiver $\mathbf{y_o}$ are expressed as follows:

$$\begin{aligned}&\mathcal{S} = \mathcal{P}R^{-\alpha}G_m(\omega, G_s)G_m(\omega, G_s),\\ &\mathcal{I} = \sum_{x_i \in \Gamma} \mathcal{P}d_i^{-\alpha}\mathcal{G}_t\left(\rho_{x_{io}}, \phi_{x_{io}}, \omega, G_s\right)\mathcal{G}_r\left(\rho_{x_{oi}}, \phi_{x_{oi}}, \omega, G_s\right),\end{aligned} \tag{12}$$

where Γ denotes the set of interferencing nodes, $\mathcal{P}$ denotes transmit power, and d_i denotes the distance between interference nodes and the typical receiver, i.e., $d_i = \|\mathbf{x_i} - \mathbf{y_o}\|$. Then, SINR is expressed as follows:

$$\text{SINR} = \frac{\mathcal{S}}{\mathcal{I} + \eta}, \tag{13}$$

where η denotes noise power.

3. Simulation results

System parameters are set to $R = d_{min} = 100\,\text{m}$, $\alpha = 2$, terrestrial service area $A = 10\,\text{km} \times 10\,\text{km}$, the number of UAVs in the terrestrial service area $\lambda A = 100$, $\omega = \{10°, 30°, 60°, 120°\}$, $G_s = 0 \sim 0.2$, $h_{min} = 50\,\text{m}$, $h_{max} = \{150\,\text{m}, 250\,\text{m}\}$, and $d_{max} = 100\,\text{m} \sim 2000\,\text{m}$. Since the path-loss exponent for air-to-air was also estimated at 2.05, we consider the free space path-loss exponent of 2 [10].

3.1. The analysis of directional antenna gain

Fig. 3 shows directional antenna gain pattern for varying G_s and ω from Eq. (9). The left plot of Fig. 3 shows the gain of main-lobe for varying G_s and ω in dB scale units. As ω is narrow, the gain of main-lobe increases. Accordingly, as G_s decreases, the gain of main-lobe increases. Let θ be the angle of the vector from location $\mathbf{x_i}$ to location $\mathbf{y_o}$ relative to the center of beam. If θ is between $-\omega/2$ and $\omega/2$, the antenna gain is $G_m(\omega)$, Otherwise G_s. The right plot of Fig. 3 shows the antenna gain of the vector with θ for ω at $G_s = 0.1$. For an

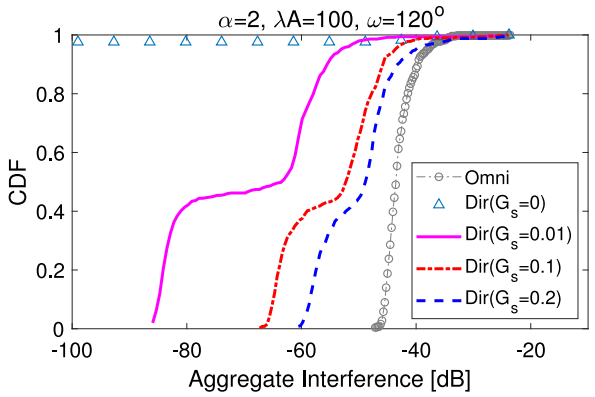

Fig. 4. CDF of aggregate interference according to G_s.

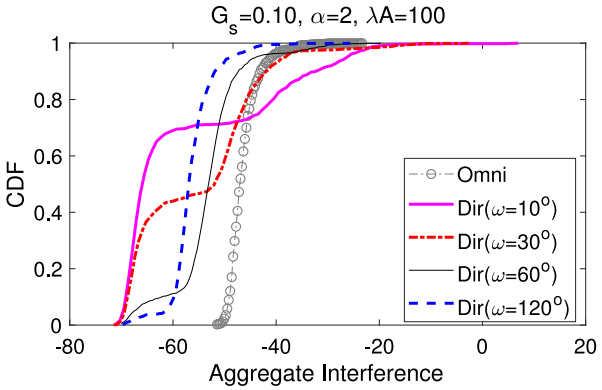

Fig. 5. CDF of aggregate interference according to ω.

example, at $\omega = 60°$, main-lobe gain of 5 db is achieved from $-30° \sim 30°$ while side-lobe gain of about 0 db is achieved from $-180° \sim -30°$ and $30° \sim 180°$.

3.2. The analysis of CDF of interference

We analyze the interference in terms of the effect of side-lobe gain, beamwidth, and the maximum height. First, we set system parameters to be $h_{max} = 150\,\text{m}$, $\alpha = 2$, $R = d_{min} = d_{max} = 100\,\text{m}$, and $\lambda A = 100$. By the condition of $R = d_{min} = d_{max}$, a pair of a typical transmitter and typical receiver retains the distance of R as well as all pairs of interferencing nodes retain the same distance of R.

Fig. 4 shows the CDF of aggregate interference according to G_s for given $\omega = 120°$. As G_s increases, the amount of interference increases due to side-lobe and the CDF of interference is shifted to the right which is the region of strong interference. For no side-lobe of $G_s = 0$, 99% of the nodes cause small interference amount less than -100 dB.

Fig. 5 shows the CDF of aggregate interference according to ω for given $G_s = 0.1$. In case of an omni antenna, the aggregate interference is between -48 dB and -25 dB. However, for $\omega = 10°$, the aggregate interference is between -70 db and 8 db. Although 70% of the aggregate interference is less than -65 dB, about 20% cause strong interference greater than -40 dB. Strong interference begins to decrease at 60° and there is no overall strong interference at 120°. Therefore, strong interference cancellation seems to be necessary for the narrow beamwidth.

Fig. 6 shows the CDF of aggregate interference at $h_{max} = 250\,\text{m}$ compared to that at $h_{max} = 150\,\text{m}$. In case of an omni antenna, there is little change in CDF of aggregate interference. When narrow beam like $\omega = 10°$ and wide beam like $\omega = 120°$, the strong interference is a little reduced caused by the increase of the maximum height. Since the narrow beam makes most of strong interference be reduced, the effect of the height increase is negligible. Additionally, since the interference is spread over most of area by wide beam, the effect of the height increase is negligible. At $\omega = 30°$ and $\omega = 60°$, the interference is improved due to increasing the maximum height. For $\omega = 30°$, the value of CDF of

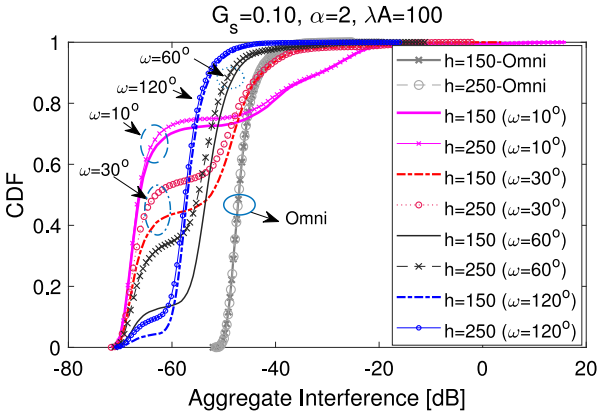

Fig. 6. CDF of aggregate interference according to h_{max}.

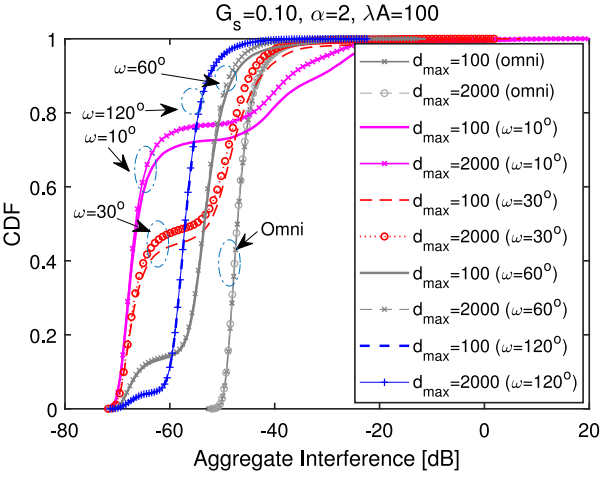

Fig. 7. CDF of aggregate interference according to d_{max}.

interference at -60 db is increased from 0.4 to 0.55. Also, for $\omega = 60°$, the value of CDF of interference at -60 db is increased from 0.15 to 0.35.

Fig. 7 shows the CDF of aggregate interference at $d_{max} = 2000\,\text{m}$ compared to that at $d_{max} = 100\,\text{m}$ for given $h_{max} = 150\,\text{m}$. As the beamwidth is narrow, the strong interference is

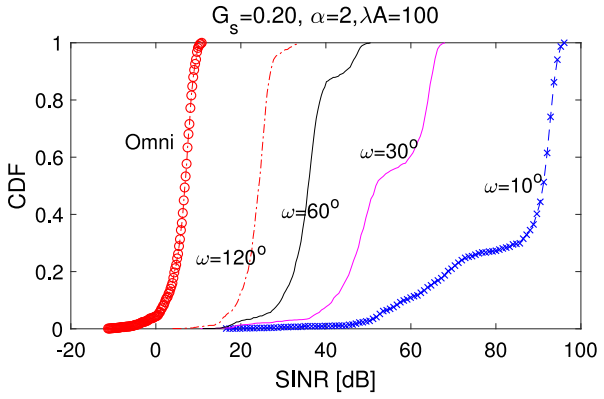

Fig. 8. CDF of SINR according to ω.

more reduced caused by the increase of d_{max}. For $\omega = 10°$, the value of CDF of interference at -60 dB is increased from 0.7 to 0.75. Also, for $\omega = 30°$, the value of CDF of interference at -60 dB is increased from 0.42 to 0.5. However, the CDF of interference slightly is improved at $\omega = 60°$. There is little effect on the increases of d_{max} in case of $\omega = 120°$ and an omni-antenna.

3.3. The analysis of SINR

Fig. 8 shows CDF of SINR according to ω for given $G_s = 0.2$, $d_{max} = 100$ m, and $h_{max} = 100$ m. For small ω, the antenna gain of the main-lobe is large as shown in Fig. 3. From this, it can be seen that the SINR increases due to a sharp increase in the desired signal. In case of $\omega = 10°$, SINR can be seen to increase sharply due to 70% weak interference and the strong desired signal.

4. Conclusions

In this paper, we showed distribution of the aggregate interference and distribution of SINR at a typical UAV receiver from multiple UAVs. From numerical results, we showed that the aggregate interference becomes significantly decreased if the beamwidth decreases or the antenna gain of side-lobe decreases. The narrower beamwidth increases the signal strength but it may induce strong interference to other UAV wireless links as well. When the height of UAV increases, the aggregate interference become decreased at the beamwidths of 30° and 60°, compared to those of 10° and 120°. Furthermore, when the distance of a pair of UAV increases, the narrower beamwidth decreases the aggregate interference. Therefore, interference management techniques and beam steering techniques are required for the directional UAV network. We leave the interference management such as interference avoidance or cancellation as well as beam steering finding the space with the least interference for the directional UAV network in a 3D space as a further study.

Acknowledgments

This research was partly supported by the National Research Foundation (NRF) of South Korea through the Basic Science Research Program funded by the Ministry of Science and ICT under Grant (NRF2019R1A2B5B01070697) and this research was partly supported by Basic Science Research Program through the NRF funded by the Ministry of Education of South Korea (NRF-2018R1A6A3A01012714).

Conflict of interest

The authors declare that there is no conflict of interest in this paper.

References

[1] H. Shakhatreh, et al., Unmanned aerial vehicles: A survey on civil applications and key research challenges, 2018, arXiv preprint arXiv:1805.00881.
[2] W. Shi, H. Zhou, J. Li, W. Xu, N. Zhang, X. Shen, Drone assisted vehicular networks: Architecture, challenges and opportunities, IEEE Netw. 32 (3) (2018) 130–137.
[3] P. Sharma, D. Kim, Coverage probability of 3-D mobile UAV networks, IEEE Wireless Commun. Lett. 8 (1) (2019) 97–100.
[4] Z. Yuan, J. Jin, L. Sun, K. Chin, C. Muntean, Ultra-reliable IoT communications with UAVs: A swarm use case, IEEE Commun. Mag. 56 (12) (2018) 90–96.
[5] Z. Xue, J. Wang, G. Ding, Cooperative data dissemination in air-ground integrated networks, IEEE Wireless Commun. Lett. 8 (1) (2019) 209–212.
[6] J. Lyu, R. Zhang, Network-connected UAV: 3D system modeling and coverage performance analysis, IEEE Internet Things J. (2019) arXiv preprint arXiv:1901.07887.
[7] Z. Zheng, A. Sangaiah, T. Wang, Adaptive communication protocols in flying ad hoc network, IEEE Commun. Mag. 56 (1) (2018) 136–142.
[8] Z. Feng, L. Ji, Q. Zhang, W. Li, Spectrum management for mmwave enabled UAV swarm networks: Challenges and opportunities, IEEE Commun. Mag. 57 (1) (2019) 146–153.
[9] E. Chu, J. Kim, B. Jung, Interference analysis of directional UAV networks: A stochastic geometry approach, in: Proc. IEEE ICUFN, Jul. 2019.
[10] N. Ahmed, S. Kanhere, S. Jha, On the importance of link characterization for aerial wireless sensor networks, IEEE Commun. Mag. 54 (5) (2016) 52–57.